THE JOURNAL OF PHYSICAL CHEMISTRY C

ARTICLE

pubs.acs.org/JPCC

Quantum Dots and Nanoroads of Graphene Embedded in Hexagonal Boron Nitride

Somnath Bhowmick,[†] Abhishek K. Singh,[†,‡] and Boris I. Yakobson*[,†]

[†]Department of Mechanical Engineering and Materials Science, Rice University, Houston, Texas 77005, United States

[‡]Materials Research Centre, Indian Institute of Science, Bangalore 560012, India

ABSTRACT: The quest for novel two-dimensional materials has led to the discovery of hybrids where graphene and hexagonal boron nitride (h-BN) occur as phase-separated domains. Using first-principles calculations, we study the energetics and electronic and magnetic properties of such hybrids in detail. The formation energy of quantum dot inclusions (consisting of n carbon atoms) varies as $1/\sqrt{n}$, owing to the interface. The electronic gap between the occupied and unoccupied energy levels of quantum dots is also inversely proportional to the length scale, $1/\sqrt{n}$—a feature of confined Dirac fermions. For zigzag nanoroads, a combination of the intrinsic electric field caused by the polarity of the h-BN matrix and spin polarization at the edges results in half-metallicity; a band gap opens up under the externally applied "compensating" electric field. For armchair nanoroads, the electron confinement opens the gap, different among three subfamilies due to different bond length relaxations at the interfaces, and decreasing with the width.

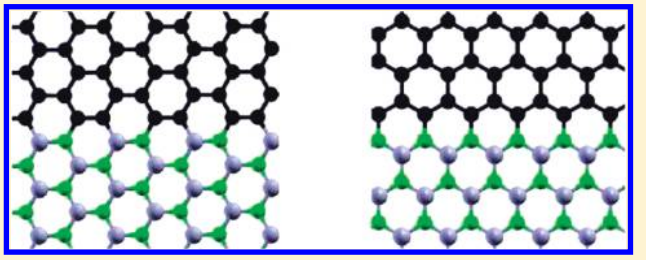

Two-dimensional materials have drawn tremendous attention in the recent past in terms of both interesting fundamental physics and possible applications in future generation devices. Graphene and hexagonal boron nitride (h-BN) are the two most promising candidates for this purpose.[1−3] Single layers of graphene and h-BN have been fabricated and found to be stable at room temperature.[4−8] The most significant difference between the two isostructured materials lies in their electrical conductivity. Whereas graphene is a semimetal and a very good conductor,[1,9] BN is an insulator (band gap $\sim$ 6 eV),[10] which limits their applications in electronic devices. This void can be bridged by combining graphene and BN to make semiconducting material with a stoichiometry of $B_xC_yN_z$.[11] Other than the solid solution of B, C, and N, it is also necessary to explore the possibility of fabricating a graphene−BN composite material, where the two phases coexist separately, but in the same plane. Such a novel composite is the focus of the present work.

Free standing nanostructures, such as nanoribbons[12,13] and quantum dots[14] (QDs) of graphene, have been discussed extensively in the literature. The effect of electron confinement leads to size-dependent electronic properties in graphene nanostructures. Interestingly, properties of graphene nanostructures are also dependent on the edge shapes, namely, zigzag (ZZ) and armchair (AC).[1] For example, the tight binding model predicts ZZ and AC nanoribbons to be metallic and seimconducting, respectively.[1,15] Density functional theory-based calculations further show that ZZ edges are spin-polarized and corresponding nanoribbons are also semiconducting in nature.[12−14] Similar properties have been reported for graphene nanoroads[16] and QDs[17] *embedded* in graphane. Fundamentally *free-standing* and *graphane-embedded* nanostructures of graphene are similar. Whereas electrons are confined by an infinite potential (due to vacuum) in the former, the latter creates a finite potential well (due to wide-band-gap graphane) for the semimetallic graphene phase.

In terms of device integration and mechanical integrity, nanoroads or QDs of graphene in a graphane matrix appear to be more promising than artificially cut freestanding nanostructures. A recent experimental discovery shows that insulating h-BN can also be used to host the graphene QDs.[18] Instead of forming a solid solution of B, N, and C, graphene and h-BN have been found to occur in separate domains inside the composite.[18] Immiscibility of the two phases has also been predicted by first-principles calculations.[19,20] In this paper, we show that such a novel material can be qualitatively different from a graphene−graphane composite due to polarity of the h-BN matrix.

It is well known that edge[14] and interface[17] shape determines the properties of free-standing and embedded graphene QDs. Thus, in this work, we consider dots of hexagonal shape, making ZZ and AC interfaces with the constituent atoms of the h-BN matrix. Two of the representative unit cells are illustrated in Figure 1. The interatomic distance between any atomic pair is 1.45 Å (equal to the bond length of BN) prior to the relaxation. Because graphene has a smaller equilibrium interatomic distance (1.42 Å), the QD after relaxation will be under tensile stress, which ensures overall planarity of the C−BN composite structure. The formation energy per atom $\varepsilon(n)$ of a graphene QD, consisting of $n(=2 \times n_C)$ carbon atoms, is defined as

$$n\varepsilon(n) = E_{tot}^{QD} - E_C n_C - E_{BN} n_{BN} \quad (1)$$

Received: January 21, 2011

   dx.doi.org/10.1021/jp200671p | *J. Phys. Chem. C* XXXX, XXX, 000–000

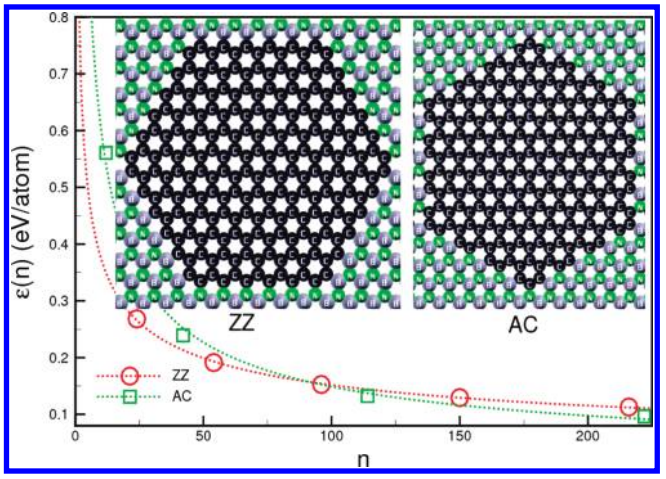

Figure 1. Formation energy of embedded graphene QDs (shown in the inset) as a function of size n.

where E_{tot}^{QD} is the total energy of the C−BN composite system consisting of n_C (n_{BN}) number of C pairs (BN pairs); E_C (E_{BN}) is the energy of a C pair in graphene (BN pair in h-BN). As shown in Figure 1, the formation energy of graphene quantum dots follows a general trend $\varepsilon(n) \sim \text{constant}/\sqrt{n}$, irrespective of the nature of the interface. This is due to the energy cost of graphene−BN interface formation, proportional to the perimeter of the graphene QD and thus scales as $\sqrt{n}$, which is divided by the QD size n, resulting in $1/\sqrt{n}$ dependence for $\varepsilon(n)$.

The interface formation energy γ determines the interface stability and equilibrium shape of QDs. Qualitatively, it is clear from Figure 1 that the armchair QDs are energetically more favorable at larger sizes. Although this hints at the possibility that γ_{AC} (armchair interface formation energy) is smaller than $\bar{\gamma}_{ZZ}$ (average of zigzag interface formation energy, to be explained later), we cannot quantify it from quantum dot-based calculations. Note that, in addition to γ, $\varepsilon(n)$ also includes strain energy (due to 2% lattice mismatch between graphene and h-BN) and hexagon corner formation energy. Though the latter does not scale with size and is insignificant for large QDs, the former cannot be neglected, because it is proportional to the area of a given graphene QD. To explicitly calculate the values of γ_{AC} and $\bar{\gamma}_{ZZ}$, the same technique as we described in ref 17 is followed. As shown in Figure 2, we form a composite nanoroad, consisting of BN and graphene single layers with a size of $L \times w$ each. The formation energy of the composite C−BN supercell can be decomposed into strain energy and interface formation energy as,

$$\frac{1}{2L}[E_{tot} - (E_C + E_{BN})N] = (Y\varepsilon^2 w/2 + \gamma) \equiv \gamma'(w) \quad (2)$$

where E_{tot} is the total energy of the supercell having N number of C and BN pairs each; E_C (E_{BN}) is the energy of a C pair in graphene (BN pair in h-BN). Y and ε are the elastic constant and strain, respectively. We keep the L fixed, and calculate $\gamma'(w)$ for various widths. As shown in Figure 2, the computed values follow a linear behavior, as expected, and the intercept gives the formation energies of the respective interfaces: $\bar{\gamma}_{ZZ}$ = 0.28 eV/Å and γ_{AC} = 0.22 eV/Å. However, because of the lack of inversion symmetry, it is not straightforward to calculate the energy of zigzag interfaces, because a ZZ nanoroad of graphene is terminated by B|C and N|C interfaces at the opposite sides (here, we report the average $\bar{\gamma}_{ZZ}$).

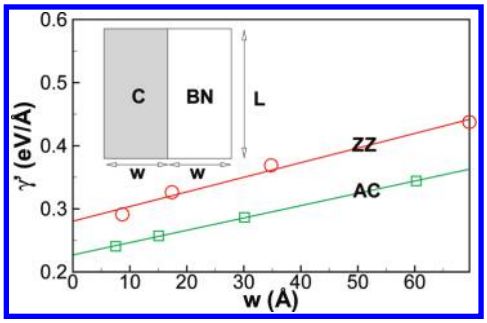

Figure 2. γ' plotted as a function of nanoroad width w. The ZZ and AC interface energy is determined from the intercept of the linear fit of the data points. Consult eq 2 for a detailed explanation.

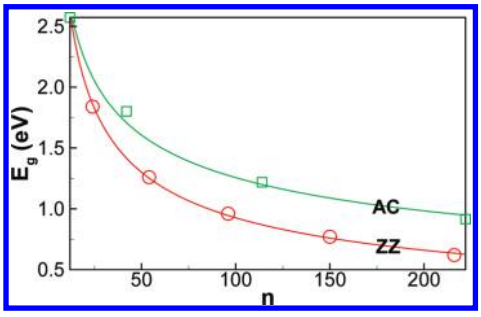

Figure 3. HOMO−LUMO gap at the Γ point, plotted for the embedded ZZ and AC graphene QDs as a function of size n.

One of the main reasons of interest in QDs is their electronic properties, which can be tuned by controlling the size of the dot. Such a feature is the manifestation of the effect of electron confinement. It is well known that graphene is a gapless material[9] and its low-energy excitations are Dirac fermion-like.[1] Confinement of Dirac electrons (by the wide-band-gap h-BN matrix) in a circular dot of radius R leads to $E_g \sim 1/R$,[21] instead of $1/R^2$ dependence for Schrödinger fermions in regular quantum dots, E_g being the energy gap between the highest occupied−lowest unoccupied molecular orbital (HOMO−LUMO gap). In Figure 3, we plot the HOMO−LUMO gap at the Γ point, obtained from first-principles calculations. Least-square fit reveals that the gap follows $E_g \sim n^{-x}$, where x is found to be 0.38 and 0.48 for AC and ZZ QDs, respectively. Approximating the hexagon by a circular QD and noting that the radius $R \sim \sqrt{n}$, we observe that the gap follows approximately $E_g \sim 1/\sqrt{n} \sim 1/R$, as expected for Dirac fermions.[21] However, such an approximation cannot explain higher E_g in AC QDs, because circular dots are terminated by a mixture of ZZ and AC edges. On the contrary, the hexagonal QDs we consider are bound purely by either ZZ or AC interfaces. Whereas electron confinement by AC edges results in a gapped energy spectrum, localized states at the ZZ edges produce partially flat bands and sharp density of states at the Fermi level.[22] However, such a metallic behavior becomes apparent above a critical size of 7−8 nm in ZZ QDs.[23] Below that (we study up to a size of 2−3 nm), they have finite E_g, which follow the power law consistent with Dirac electron confinement.[23] The distinct trend observed in Figure 3 reflects the near metallic nature of large ZZ QDs compared to AC QDs of the same size.

In view of the possible applications of these QDs in electronic devices, it is important to determine the quality of the interfaces

dx.doi.org/10.1021/jp200671p |J. Phys. Chem. C XXXX, XXX, 000–000

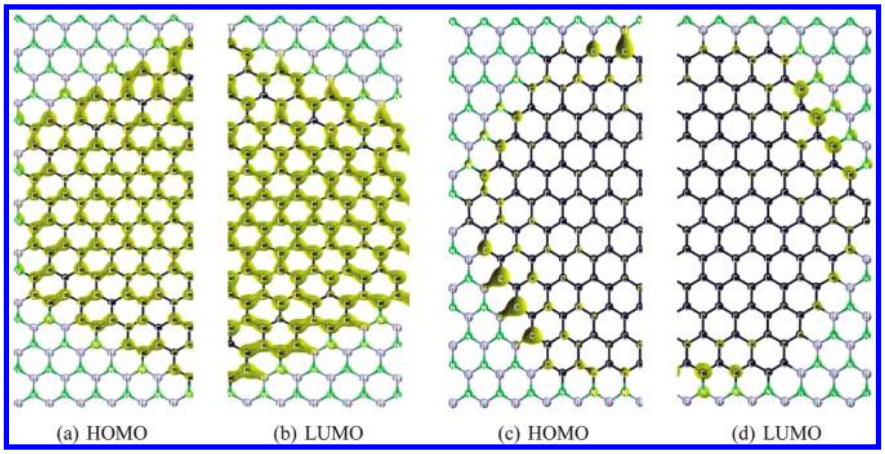

Figure 4. Band decomposed electron densities of the HOMO and LUMO of (a, b) AC and (c, d) ZZ graphene QDs embedded in h-BN. For AC QDs, the charge density of the HOMO and LUMO is uniformly spread over the entire dot. For ZZ QDs, the HOMO and LUMO charge density is localized at the B- and N-terminated edges, respectively.

in terms of electron confinement. From the band decomposed electron densities of the HOMO and LUMO, as shown in Figure 4, it is clear that "leakage" to the BN phase is negligible. The charge density of the HOMO and LUMO is spread over the entire dot of the AC QD (Figure 4a,b). On the other hand, the same quantity is localized at the edges in the ZZ QD (Figure 4c,d). Such electron densities are due to the edge states formed by the π electrons of C, previously observed in hydrogen-terminated zigzag graphene nanoribbons or QDs.[1,22] As mentioned before, diatomic BN forms two inequivalent classes of zigzag interfaces with graphene, terminated by either B or N. This lowers the symmetry of a hexagonal graphene QD in BN, where HOMO and LUMO charge densities are localized at the B- and N-terminated edges, respectively (see Figure 4c,d).

The existence of edge localized states in ZZ-terminated graphene nanostructures result in spin-polarized edges.[1] For example, magnetism is predicted in free-standing hexagonal ZZ QDs of graphene above a critical size.[14] We expect similar features in hexagonal ZZ graphene QDs embedded in h-BN. However, even the largest of the QDs in our calculation are below the threshold size for the onset of magnetism, as reported in the literature.[14] The computations are expensive because not only do we have to deal with a larger graphene QD but also we have to include the BN matrix, effectively making the system too large. Thus, we shift our focus to nanoroads, a relatively small system, although it captures all the essential physics.

On the basis of first-principles calculations, magnetism in hydrogen-terminated freestanding zigzag nanoribbons has been discussed in detail by Son et al.[12,13] The magnetic moments are localized at the zigzag edges, arranging themselves ferromagnetically along a particular edge. Of all the possible magnetic configurations, the one where two opposite edges are coupled antiferromagnetically has the lowest energy.[12,13] Staggered sublattice potential generated due to the magnetic ordering opens up a band gap, which also depends on the ribbon width.[12] A similar effect has been observed in graphene nanoroads embedded in graphane.[16] Zigzag graphene nanoroads in hexagonal boron nitride have similar magnetic orientations (shown in Figure 5a). Down (up) spin density is mostly localized at the C atom, making an interface with N (B), at the two opposite boundaries of the graphene nanoroad. Interestingly, the band structure

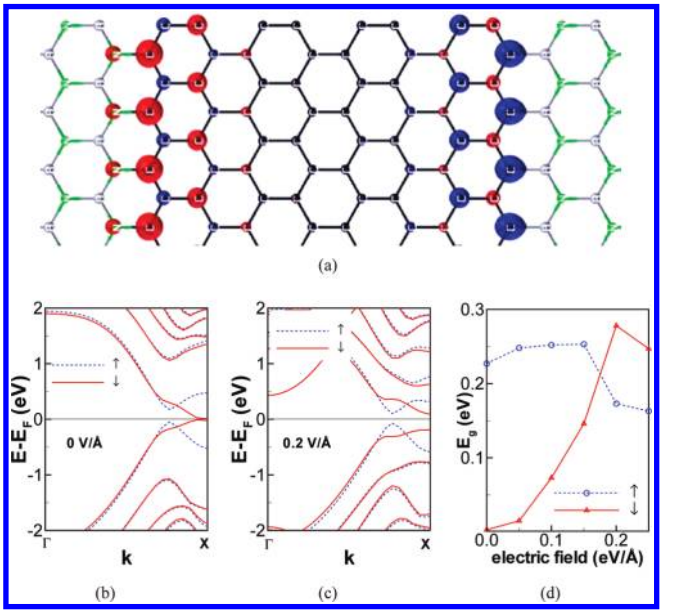

Figure 5. (a) The spin density of a graphene nanoroad embedded in h-BN. Red and blue correspond to down and up spin density, respectively. Band structure of the same nanoroad in (b) zero electric field and (c) an externally applied electric field. The system changes from half-metallic to semiconducting in a finite field, applied across the NC to the BC interface. (d) Band gap of both the spins as a function of applied field.

(shown in Figure 5b) resembles that of a half-metallic system. Whereas the down spin electrons are metallic, a direct band gap exists for the up spin electrons.

Half-metallicity has been reported in graphene nanoribbons in an external electric field, applied across the ribbon width.[13] As shown here, a carefully designed graphene−BN composite eliminates the need of an external electric field to achieve a half-metallic material. This is the most spectacular manifestation of the effects of polarity of BN on the electronic properties of C−BN composites. The two edges of the graphene nanoroad are at different electrostatic potentials, which produces an effective electric field, directed from the B|C interface to the N|C interface. To verify this hypothesis, we perform the following Gedanken experiment. We apply an external electric field in

dx.doi.org/10.1021/jp200671p |J. Phys. Chem. C XXXX, XXX, 000–000

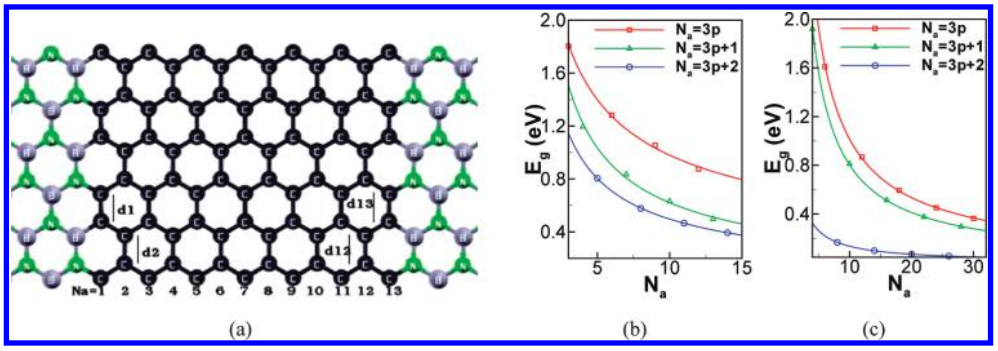

Figure 6. (a) Graphene nanoroad having an armchair interface with the BN phase. N_a is the number of C−C dimers along the nanoroad width. d_1, d_2... are the bond lengths of the respective dimers. Band gap, obtained from (b) DFT and (c) tight binding calculations, plotted as a function of nanoroad width of an armchair graphene nanoroad embedded in BN.

the direction (along the N|C to B|C interface) reverse to the effective intrinsic field. As shown in Figure 5c, the "compensating" field indeed opens up a direct energy gap at the X-point to the otherwise gapless down spin band. The band gaps as a function of applied field are shown in Figure 5d. Both spins have similar E_g (∼0.2 eV, at the X-point for down spin and away from the X-point for up spin) in an external electric field of 0.15−0.20 eV/Å. An electric field of a similar strength has been reported to produce half-metallicity in zigzag graphene nanoribbons.[13] It is difficult to apply such a huge electric field in practice. In principle, it is more realistic to design an intrinsic half-metal, made of a composite of graphene and BN, where the polarity of the latter naturally creates an effective electric field across the graphene nanoroad. We have investigated nanoroads with a width of 2−4 nm, all of which show similar half-metallic behavior. Although the intrinsic electric field weakens with increasing nanoroad width, the electrostatic potential difference (field times the width) between the two interfaces of the zigzag graphene nanoroad remains strong enough to induce half-metallicity. A similar dependence has been reported for zigzag graphene nanoribbons, where the critical external field required for half-metallicity has been found to be inversely proportional to the ribbon width.[13]

Finally, we briefly discuss armchair graphene nanoroads embedded in h-BN. Such a structure has been shown in Figure 6a, N_a being the number of C−C dimers along the width of the nanoroad, and d_1, d_2... are corresponding bond lengths. Armchair graphene nanoroads can be classified into three families with a gap $\sim 1/N_a$ for each one of them. As shown in Figure 6b, the gap size follows the order of $E_g(3p) > E_g(3p + 1) > E_g(3p + 2)$, which is distinct from armchair graphene nanoribbons,[12] but similar to armchair graphene nanoroads in graphane.[16] Whereas the $E_g(3p + 2)$ family has the smallest gap, in the case of both armchair nanoribbons and nanoroads, $E_g(3p)$ and $E_g(3p + 1)$ occur in an opposite sequence.[12] We perform a simple tight binding analysis to understand this, using the following Hamiltonian

$$H = -t \sum_{\langle i,j \rangle} c_i^\dagger c_j + \text{h.c.} \qquad (3)$$

where t is the nearest-neighbor hopping integral, $c_i^\dagger$ (c_j) creates (annihilates) an electron at site i (j), and h.c. is the Hermitian conjugate. From first-principles calculations, t has been found to be 2.7 eV for an equilibrium interatomic distance of 1.42 Å among C atoms in graphene.[24] However, t is modified as the C−C bond length changes from its equilibrium value.[25] Using first-principles-based structural relaxation, we find that the smallest and largest C−C distance in an embedded AC graphene nanoroad is $d_1 = d_{13} = 1.42$ Å and $d_2 = d_{12} = 1.46$ Å, respectively. The rest of the C−C bond lengths lie in the range of 1.42−1.44 Å. On the basis of this observation, we choose the simplest model where the hopping integral of the atoms connected by d_2 and d_{12} are taken to be $0.9t$. The reduced value accounts for the enhanced bond length. The rest of the hopping integrals are kept at their equilibrium value of 2.7 eV. As shown in Figure 6c, the model correctly captures the hierarchy for the band gaps of the family of AC graphene nanoroads embedded in h-BN.

In conclusion, we have investigated the formation energy and electronic and magnetic properties of selected QDs and nanoroads of graphene embedded in h-BN. AC QDs and nanoroads have a lower formation energy than that of ZZ. Dots and AC nanoroads are semiconducting with a tunable band gap (by controlling the size) and are suitable for optoelectronic applications. ZZ nanoroads of graphene possess spin-polarized edges, making an interface with the h-BN matrix. Because of the polarity of h-BN, two opposite interfaces of a ZZ graphene nanoroad are at different electrostatic potentials, creating an intrinsic electric field across the width of the nanoroad. This results in half-metallicity, and a band gap can be opened and tuned under the influence of an externally applied electric field, ideal for the purpose of fabricating spin transport devices, such as spin valves, magnetic tunnel junctions, magnetoresistive random access memory (MRAM), etc.[26] We further note that a recent important development[27] allows one to separate and clearly define the energies of the opposite ZZ edges of BN or its interfaces (γ_{ZZ-B} and γ_{ZZ-N} instead of just their sum-average, γ_{ZZ}) so that the edge energy and the Wulff construction can be computed for arbitrary direction,[28] to determine their dependencies on the chemical potential of B or N and, therefore, to suggest possible control of the 2D morphology and physical properties.[27]

METHOD

We use density functional theory (DFT)-based first-principles calculations as implemented in the PWSCF code[29] with a plane-wave basis set and ultrasoft pseudopotentials. Electron exchange and correlation is treated within a framework of Perdew−Burke−Ernzerhof[30] generalized gradient approximation (GGA). We set the kinetic energy cutoff for wave functions to be 40 Ry. We use supercell geometry with a vacuum of ∼15 Å in "nonperiodic" directions to decouple the interaction between two images. In all the QD calculations, the Brillouin zone is

dx.doi.org/10.1021/jp200671p |J. Phys. Chem. C XXXX, XXX, 000–000

represented by the Γ point. A *k*-point grid of 48(24) × 2 × 1 is used to sample the Brillouin zone of the ZZ (AC) nanoroads. We relax the structures fully until the force on each atom (total energy change for ionic minimization) is less than 10^{-3} Ry/au (10^{-4} Ry).

AUTHOR INFORMATION

Corresponding Author
*E-mail: biy@rice.edu.

ACKNOWLEDGMENT

This work was supported by the Department of Energy, BES (Grant No. ER46598), and partially (A.K.S., analysis of spin polarization) by the Office of Naval Research, MURI. The computations were performed on Kraken, at the National Institute for Computational Sciences, through allocation TG-DMR100029.

REFERENCES

(1) Neto, A. H. C.; Guinea, F.; Peres, N. M. R.; Novoselov, K. S.; Geim, A. K. *Rev. Mod. Phys.* **2009**, *81*, 109.
(2) Geim, A. K.; Novoselov, K. S. *Nat. Mater.* **2007**, *6*, 183–191.
(3) Golberg, D.; Bando, Y.; Huang, Y.; Terao, T.; Mitome, M.; Tang, C.; Zhi, C. *ACS Nano* **2010**, *4*, 2979–2993.
(4) Novoselov, K. S.; Jiang, D.; Schedin, F.; Booth, T. J.; Khotkevich, V. V.; Morozov, S. V.; Geim, A. K. *Proc. Natl. Acad. Sci. U.S.A.* **2005**, *102*, 10451.
(5) Meyer, J. C.; Geim, A. K.; Katsnelson, M. I.; Novoselov, K. S.; Booth, T. J.; Roth, S. *Nature* **2006**, *446*, 60–63.
(6) Gass, M. H.; Bangert, U.; Bleloch, A. L.; Wang, P.; Nair, R. R.; Geim, A. K. *Nat. Nanotechnol.* **2008**, *3*, 676–681.
(7) Jin, C.; Lin, F.; Suenaga, K.; Iijima, S. *Phys. Rev. Lett.* **2009**, *102*, 195505.
(8) Nag, A.; Raidongia, K.; Hembram, K. P. S. S.; Datta, R.; Waghmare, U. V.; Rao, C. N. R. *ACS Nano* **2010**, *4*, 1539–1544.
(9) Wallace, P. R. *Phys. Rev.* **1947**, *71*, 622–634.
(10) Blase, X.; Rubio, A.; Louie, S. G.; Cohen, M. L. *Phys. Rev. B* **1995**, *51*, 6868–6875.
(11) Liu, A. Y.; Wentzcovitch, R. M.; Cohen, M. L. *Phys. Rev. B* **1989**, *39*, 1760–1765.
(12) Son, Y. W.; Cohen, M. L.; Louie, S. G. *Phys. Rev. Lett.* **2006**, *97*, 216803.
(13) Son, Y. W.; Cohen, M. L.; Louie, S. G. *Nature* **2006**, *444*, 347–349.
(14) Fernández-Rossier, J.; Palacios, J. J. *Phys. Rev. Lett.* **2007**, *99*, 177204.
(15) Brey, L.; Fertig, H. A. *Phys. Rev. B* **2006**, *73*, 235411.
(16) Singh, A. K.; Yakobson, B. I. *Nano Lett.* **2009**, *9*, 1540–1543.
(17) Singh, A. K.; Penev, E. S.; Yakobson, B. I. *ACS Nano* **2010**, *4*, 3510–3514.
(18) Ci, L.; Song, L.; Jin, C.; Jariwala, D.; Wu, D.; Li, Y.; Srivastava, A.; Wang, Z. F.; Storr, K.; Balicas, L.; Liu, F.; Ajayan, P. M. *Nat. Mater.* **2010**, *9*, 430–435.
(19) Yuge, K. *Phys. Rev. B* **2009**, *79*, 144109.
(20) da Rocha Martins, J.; Chacham, H. *ACS Nano* **2011**, *5*, 385–393.
(21) Peres, N. M. R.; Rodrigues, J. N. B.; Stauber, T.; dos Santos, J. M. B. L. *J. Phys.: Condens. Matter* **2009**, *21*, 344202.
(22) Fujita, M.; Wakabayashi, K.; Nakada, K.; Kusakabe, K. *J. Phys. Soc. Jpn.* **1996**, *65*, 1920–1923.
(23) Ritter, K. A.; Lyding, J. W. *Nat. Mater.* **2009**, *8*, 235–242.
(24) Reich, S.; Maultzsch, J.; Thomsen, C.; Ordejón, P. *Phys. Rev. B* **2002**, *66*, 035412.
(25) Ribeiro, R. M.; Pereira, V. M.; Peres, N. M. R.; Briddon, P. R.; Neto, A. H. C. *New J. Phys.* **2009**, *11*, 115002.
(26) Wolf, S. A.; Awschalom, D. D.; Buhrman, R. A.; Daughton, J. M.; von Molnar, S.; Roukes, M. L.; Chtchelkanova, A. Y.; Treger, D. M. *Science* **2001**, *294*, 1488–1495.
(27) Liu, Y.; Bhowmick, S.; Yakobson, B. I., arXiv:1101.4457v1 2011.
(28) Liu, Y.; Dobrinsky, A.; Yakobson, B. I. *Phys. Rev. Lett.* **2010**, *105*, 235502.
(29) Giannozzi, P.; *J. Phys.: Condens. Matter* **2009**, *21*, 395502.
(30) Perdew, J. P.; Burke, K.; Ernzerhof, M. *Phys. Rev. Lett.* **1996**, *77*, 3865–3868.